AGU PUBLICATIONS

Space Weather

RESEARCH ARTICLE
10.1002/2016SW001401

Special Section:
Initial Results from the NASA Radiation Dosimetry Experiment (RaD-X) Balloon Flight Mission

Evaluating galactic cosmic ray environment models using RaD-X flight data

R. B. Norman[1], C. J. Mertens[1], and T. C. Slaba[1]

[1] Langley Research Center, National Aeronautics and Space Administration, Hampton, Virginia, USA

Abstract Galactic cosmic rays enter Earth's atmosphere after interacting with the geomagnetic field. The primary galactic cosmic rays spectrum is fundamentally changed as it interacts with Earth's atmosphere through nuclear and atomic interactions. At points deeper in the atmosphere, such as at airline altitudes, the radiation environment is a combination of the primary galactic cosmic rays and the secondary particles produced through nuclear interactions. The RaD-X balloon experiment measured the atmospheric radiation environment above 20 km during 2 days in September 2015. These experimental measurements were used to validate and quantify uncertainty in physics-based models used to calculate exposure levels for commercial aviation. In this paper, the Badhwar-O'Neill 2014, the International Organization for Standardization 15390, and the German Aerospace Company galactic cosmic ray environment models are used as input into the same radiation transport code to predict and compare dosimetric quantities to RaD-X measurements. In general, the various model results match the measured tissue equivalent dose well, with results generated by the German Aerospace Center galactic cosmic ray environment model providing the best comparison. For dose equivalent and dose measured in silicon, however, the models were compared less favorably to the measurements.

Key Points:
- Upper atmospheric dosimetry measurements were compared to calculations using three galactic cosmic ray models
- The three galactic cosmic ray models reproduced the dose in tissue measurements well but overpredicted measurements for dose equivalent
- Dose equivalent was found to be strongly altitude dependent, signaling the breakup of the primary galactic cosmic ray spectrum

Correspondence to:
R. B. Norman,
Ryan.B.Norman@nasa.gov

Citation:
Norman, R. B., C. J. Mertens, and T. C. Slaba (2016), Evaluating galactic cosmic ray environment models using RaD-X flight data, *Space Weather*, *14*, 764–775, doi:10.1002/2016SW001401.

Received 19 APR 2016
Accepted 21 SEP 2016
Accepted article online 28 SEP 2016
Published online 12 OCT 2016

1. Introduction

The International Commission on Radiological Protection classifies commercial aircraft crew as radiation workers [*International Commission on Radiological Protection*, 1991]. A review of monitored terrestrial radiation workers with recordable doses in 2006 found that flight crews had the largest average effective dose of any group of radiation workers [*National Council on Radiation Protection and Measurements* (*NCRP*), 2009]. Aircraft crews, however, are the only occupational group exposed to unquantified and undocumented levels of radiation in the United States. Additionally, the public and prenatal radiation exposure limits may be exceeded during a single solar storm for commercial passengers on intercontinental or polar routes, or by frequent flyers of these routes due to only the background galactic cosmic rays (GCR) environment [*Copeland et al.*, 2008; *Dyer et al.*, 2009; *Mertens et al.*, 2012].

To address the concern of unquantified radiation levels for aircrews, NASA developed the Nowcast of Atmospheric Ionizing Radiation for Aviation Safety (NAIRAS) model [*Mertens et al.*, 2010, 2012, 2013]. NAIRAS is a real-time, global, physics-based model of the ionizing radiation environment throughout the atmosphere that accounts for both GCR and solar energetic particles (SEP), the two main sources of space radiation. GCR are a low-intensity, high-energy background radiation which comes from outside the solar system and is modulated by the magnetic field of the Sun and the geomagnetic field of the Earth. SEP events are episodic eruptions of energetic particles from the Sun and are typically larger in intensity but lower in energy compared to the GCR environment.

NAIRAS uses real-time data to characterize the radiation environment, the geomagnetic field, and the atmospheric conditions on a 1° by 1° latitude and longitude grid across the entire globe. The deterministic space radiation transport suite HZETRN [*Wilson et al.*, 1991; *Slaba et al.*, 2010a, 2010b] is then used to transport the radiation field and subsequent reaction products resulting from nuclear collisions throughout the entire atmospheric column. In the end, the radiation environment throughout the global atmosphere is characterized, and the dose rate along a given radiation route can be determined. This allows both a real-time analysis of the current radiation environment along any aviation route and for the history of radiation exposure of any aircraft crew member to be tracked.

Transitioning NAIRAS from a research-level model to an operations-level model requires model validation against dosimetric measurements at aviation altitudes and estimation of model uncertainty. Initial work was conducted by *Mertens et al.* [2013] that compared NAIRAS to dosimetric data. Using the International Commission on Radiological Units (ICRU) criteria for acceptable levels of total uncertainty in radiation protection measurements and assessments of dose [*International Commission on Radiological Units*, 1992, 2001, 2010], NAIRAS met the ICRU criteria for the GCR environment. However, quantifying model uncertainty required additional effort.

To better understand the total uncertainty found in NAIRAS, measurements above commercial aviation altitudes are needed to help determine the source of uncertainty at aviation altitudes. While a significant amount of data exist for dosimetry at aircraft altitudes [*Lindborg et al.*, 2004; *Ploc et al.*, 2013], the data available above those altitudes are minimal. To address this issue, the NASA mission RaD-X was created. Experimental data above the Regener-Pfotzer [*Regener and Pfotzer*, 1934] maximum supplied NAIRAS with important information that was previously unavailable and helped model developers understand the sources of uncertainty in the models.

The RaD-X mission launched from Ft. Sumner, New Mexico, USA, (34°N, 104°W) on 25 September 2015. The four dosimeters onboard RaD-X each collected over 20 h of science data. RaD-X operated in Region B, which was defined to be above 32.5 km, for just over 6.5 h. At sunset, the balloon dropped in altitude, and an operational valve down was initiated to further drop the balloon lower in the atmosphere. RaD-X then floated in Region A, defined to be between 21.0 and 27.0 km, overnight and into the morning of 26 September 2015 for another 8.3 h.

One of the four dosimeters flown on RaD-X was a Hawk version 3.0 tissue equivalent proportional counter (TEPC) microdosimeter manufactured by Far West Technologies. The TEPC emulates the energy deposited in tissue by using a tissue equivalent plastic surrounding a propane gas detector. The TEPC measures the energy deposited in the detector as well as spectral lineal energy loss as the radiation traverses the detector. The spectrometer stores the lineal energy loss in a low-resolution component of 1024 channels from 0 to 1536 keV/μm and in a higher-resolution component for the low lineal energy with 256 channels from 0 to 25.6 keV/μm. The TEPC is the de facto industry standard for microdosimetry.

The Liulin-6SA1 linear energy transfer (LET) spectrometer manufactured at the Space Research and Technology Institute of the Bulgarian Academy of Sciences was also flown [*Dachev et al.*, 2011]. The silicon-based Liulin spectrometer has an LET range of 0–69.4 keV/μm and can detect very low dose rates down to 5.6 nGy/h. Compared to the detection volume of the TEPC, the Liulin is small and largely insensitive to neutrons. For the RaD-X mission measurements above the Regener-Pfotzer maximum, the secondary neutron field should be smaller than the proton field at all altitudes and should be minimal in Region B.

The other two detectors, a Teledyne Total Ionizing Dose detector and a Raysure detector, satisfied a secondary science goal of RaD-X—to improve understanding of the relationship between silicon-based radiation measurements and radiobiological response. This paper will focus on the TEPC and Liulin measurements.

The paper is organized as follows. Section 2 introduces and compares the three GCR models considered, section 3 compares dosimetric calculations using the three GCR models to the RaD-X measurements, and section 4 contains some concluding remarks.

2. Galactic Cosmic Ray Models

Galactic cosmic ray models are an important input into radiation transport models as the GCR models provide the boundary condition of GCR particles that is transported through materials and, along with other physics models such as atomic cross sections and nuclear cross sections, ultimately determine the number and type of particles present at a given position within the material. Figure 1 shows a simplified flow chart of the models used to generate radiation dose in the atmosphere. The transport model takes the radiation boundary condition, specified by the GCR model, and transports it through the atmosphere, which is specified by the atmosphere model. The radiation environment is altered through interactions between the radiation and the atmosphere. These interactions are specified by the physics cross-section models. Once the radiation is transported to the point of interest in the atmosphere, the transport model specifies the spectral flux of particles at that point. This flux can be converted to other response functions (e.g., dose and dose equivalent) as desired.

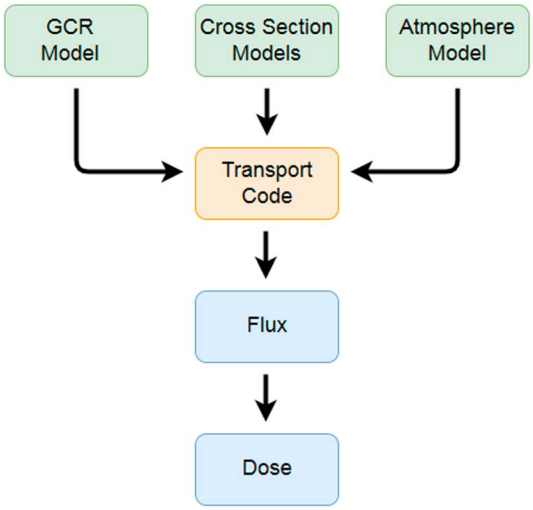

Figure 1. A simplified graphical representation of the models used in an atmospheric transport calculation.

The details of the NAIRAS model are discussed in *Mertens et al.* [2012, 2013].

Galactic cosmic ray transport in the atmosphere begins with specifying the spectrum of GCR particles near Earth. This is the boundary condition for radiation transport. GCR models typically specify a range of nuclei, starting from hydrogen and progressing to more massive elements. The spectrum of particles needs to cover the range of energies appropriate for the application. For atmospheric transport, energies extending up to 1 TeV/nucleon were found to be sufficient [*Norman et al.*, 2012, 2013].

Some GCR models solve a steady state, convective-diffusive transport equation to specify the spectral flux of fully ionized nuclear isotopes ranging from hydrogen to nickel at 1 AU [*O'Neill et al.*, 2015]. Alternatively, a more parametric model can be used which defines the particle spectrum at 1 AU directly, as is the case for the International Organization for Standardization (ISO) 15390 and DLR models [*International Organization for Standardization* (*ISO*), 2004; *Matthiä et al.*, 2013]. Each model is discussed in more detail below.

2.1. Badhwar-O'Neill 2014 Model

In the Badhwar-O'Neill 2014 (BO2014) model [*O'Neill et al.*, 2015], a radially symmetric transport equation through the heliosphere is assumed,

$$\frac{\partial}{\partial r}(r^2 U) - \frac{2r}{3}\frac{\partial}{\partial E}(E\Gamma(E)U) - \frac{\partial}{\partial r}\left[\kappa(r,E,t)r^2\frac{\partial U}{\partial r}\right] = 0. \tag{1}$$

U is the differential number density of the GCR ions with respect to the kinetic energy per nucleon E, and r is the radial distance from the sun. $\Gamma(E)$ is given by

$$\Gamma(E) = \frac{E+2m}{E+m}, \tag{2}$$

where m is the rest mass energy per nucleon of the ion. The radial diffusion coefficient $\kappa(r,E,t)$ is parameterized as

$$\kappa(r,E,t) = \frac{\kappa_0 \beta R(E)}{V_s \phi(t)}\left[1+\left(\frac{r}{r_0}\right)^2\right], \tag{3}$$

where κ_0 is the diffusion constant (1.6×10^{21} cm^2/s), β is the ratio of the charged particle's speed to the speed of light in vacuum, and $R(E)$ is the magnetic rigidity in MV (megavolts) of the ion which is related to the energy and charge of the ion. Magnetic rigidity is the momentum per unit charge of an ion. V_s is the solar wind speed that is assumed to be a constant 400 km/s, $\phi(t)$ is the solar modulation potential parameter in units of MV, r is the distance from the Sun in astronomical units (AU), and r_0 is a constant given as 4 AU. The time dependence of the model is parameterized through the solar modulation potential, which is further related to the International Sunspot Number (ISSN) [*O'Neill et al.*, 2015] as a proxy for the magnetic strength of the sun. Details of the derivation and solution of equation (1) are given in *Mertens et al.* [2013].

In addition, the local interstellar spectrum (LIS) of particles outside the heliosphere must be defined. The BO2014 model assumes a three-parameter model of the LIS spectrum for each ion [*O'Neill et al.*, 2015]. With the 2014 version of the Badhwar-O'Neill model, the parameters used to define the LIS spectrum for each of the 28 ions from hydrogen to nickel have been optimized so that the model fits experimental measurements of GCR ions within the heliosphere [*O'Neill et al.*, 2015]. Special emphasis is given to high energies as these particles are more penetrating in shielding [*Slaba and Blattnig*, 2014a].

2.2. ISO 15390 Model

The semiempirical International Organization for Standardization (ISO) model [*ISO*, 2004] is based on models developed at Moscow State University [*Nymmik and Suslov*, 1995; *Nymmik et al.*, 1996]. The ISO model begins by parameterizing the GCR spectral flux of ions at 1 AU as a function of rigidity

$$\Phi_i(R,t) = \frac{C_i \beta^{\alpha_i}}{R^{\gamma_i}} \left[\frac{R}{R + R_0(R,t)} \right]^{\Delta_i(R,t)}, \tag{4}$$

where C_i, α_i, and γ_i are parameters for GCR ions labeled by type i. R is the rigidity of the GCR ion in GV. $\Delta_i(R,t)$ and $R_0(R,t)$ are functions which describe the modulation of the GCR by the sun.

$R_0(R,t)$ is parameterized as

$$R_0(R,t) = 0.37 + 3 \times 10^{-4} \times W(t, \Delta t(R,t))^{1.45}, \tag{5}$$

where $W(t, \Delta t(R,t))$ is the ISSN number that includes a time lag ($\Delta t(R,t)$ between observed sunspots and intensity of GCR observed at Earth as described in *Nymmik et al.* [1996] and *ISO* [2004]. $\Delta_i(R,t)$ is a dimensionless parameter which depends on β, R, $R_0(R,t)$ and accounts for the relative strength of the Sun's magnetic field at time t compared to the largest and smallest solar activity of the closest two solar cycles along with the polarity of the magnetic field of the Sun [*ISO*, 2004]. Additional details can be found in the ISO standard [*ISO*, 2004], *Nymmik and Suslov* [1995], and *Nymmik et al.* [1996]. With all parameters defined, equation (4) can be used to calculate the spectral flux density used in the radiation transport model.

2.3. DLR Model

The German Aerospace Center (DLR) model is a modification of the ISO model based on the work of *Matthiä et al.* [2013]. The DLR model starts from the ISO model but treats the ISSN in equation (5) as a rigidity-independent free parameter that is fit to neutron monitor and GCR measurements. In addition, the $\Delta_i(R,t)$ parameter in equation (4) is consider to only be a linear function of the rigidity-independent ISSN, W,

$$\Delta(t) = c + bW(t). \tag{6}$$

Now equation (4) becomes

$$\Phi_i(R,t) = \frac{C_i \beta^{\alpha_i}}{R^{\gamma_i}} \left[\frac{R}{R + 0.37 + 3 \times 10^{-4} \times W(t)^{1.45}} \right]^{c+bW(t)} \tag{7}$$

in the DLR model. The parameters, in equation (6), c and b were found to be 4.7 and 0.02, respectively, through comparison to carbon measurements on board the Advanced Composition Explorer (ACE) spacecraft by the Cosmic Ray Isotope Spectrometer (CRIS) instrument [*Matthiä et al.*, 2013]. One can then derive $W(t)$, from the ACE/CRIS data. An alternative method, and one that is more applicable to the RaD-X mission, that was investigated by *Matthiä et al.* [2013] is to derive $W(t)$ based on Oulu neutron monitor count rates. By comparing the $W_{\mathrm{ACE}}(t)$ values to Oulu neutron monitor count rates, a linear model was developed which showed good correlation

$$W_{\mathrm{Oulu}} = -0.093 C_r + 638.7, \tag{8}$$

where C_r is the Oulu neutron monitor count rate in units of minutes^{-1}. Now the time dependence in equations (6) and (7) is tied to the Oulu neutron monitor count rate through equation (8).

2.4. Model Calibration

All of these models are fit in some way to available satellite and balloon measurements of the GCR environment. The largest component of the available measurement data set is the CRIS instrument on the ACE satellite [*Stone et al.*, 1998]. The ACE/CRIS measurements account for over 80% of the available data used to tune the GCR models [*Slaba and Blattnig*, 2014a]. The ACE/CRIS instrument has been measuring heavy ion flux (ions with charge $Z = 5–28$) with energies below 500 MeV/nucleon since 1997. Various other assets have measured light ions and higher energy heavy ions but for only short time periods. The limited measurements were shown to lead to a calibration bias, in which the models are found to be reasonably accurate (less than 15% model error) [*NCRP*, 2006] when compared to the available data, but larger differences (> 50%) in

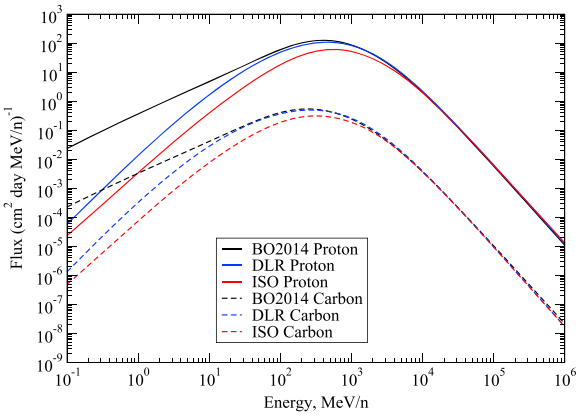

Figure 2. Differential flux of protons and carbon ions for the RaD-X flight (25–26 September 2015) from the three GCR models considered. This is the free space spectrum at 1 AU outside Earth's magnetosphere.

radiation exposure calculations behind shielding using the GCR models were found [*Mrigakshi et al.*, 2013; *Slaba and Blattnig*, 2014a]. The discovery of the calibration bias has led to more rigorous sensitivity analysis and validation [*Slaba and Blattnig*, 2014b; *Slaba et al.*, 2014]. The validation work will be aided by future improved measurements with the Alpha Magnetic Spectrometer instrument on the International Space Station [*Aguilar et al.*, 2015].

2.5. Comparison of the Models

Figure 2 shows a comparison of the three GCR model results for the differential flux of protons and carbon ions outside Earth's magnetosphere for the dates of 25–26 September 2015 corresponding to the RaD-X flight. The ISO model output was taken from the SPENVIS website (https://www.spenvis.oma.be) and interpolated/extrapolated onto the same energy grid used for the other two models. The dates of the RaD-X flight were used as input to SPENVIS to obtain the differential flux of GCR ions from protons to nickel. For the DLR model, the average count rate corrected for efficiency and pressure for the Oulu neutron monitor (http://cosmicrays.oulu.fi/) was found to be 6211.42 min^{-1}. This resulted in $W_{\text{Oulu}} = 61.04$ from equation (8), which was used as input to the DLR model.

The International Sunspot Number was updated [*Clette et al.*, 2014] prior to the RaD-X flight. However, the BO2014 model was tuned to the previous version of the ISSN. To allow use of the new ISSN data, an average scaling factor was determined by looking at the last 2 years of ISSN. An average multiplicative value of 1.44 was needed to bring the updated ISSN values in line with the previous version. This was necessary to allow the BO2014 model to be used for the RaD-X flight dates. The sensitivity of the dose rate behind moderate shielding using the BO2014 was found to be less than 1% given a 20% variation in the ISSN.

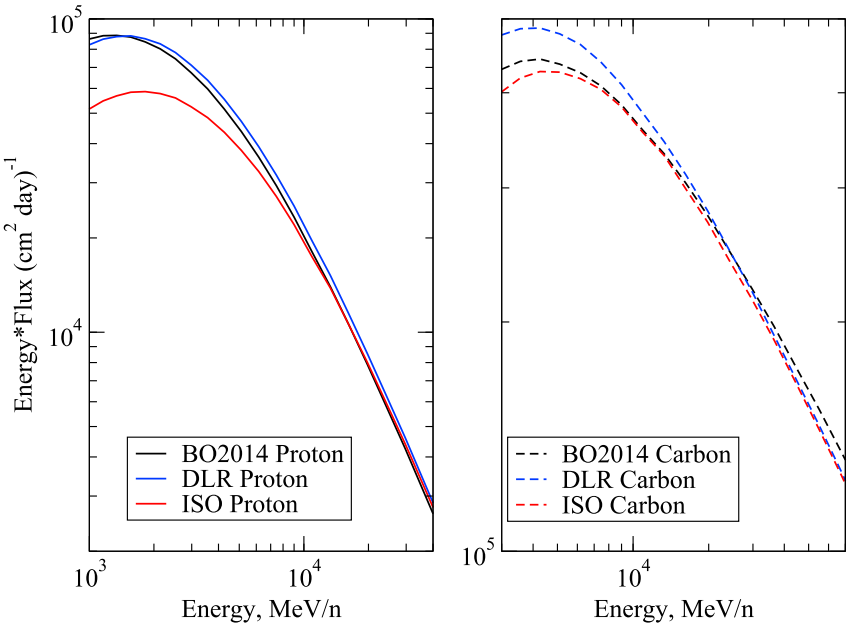

Figure 3. The high-energy component of protons and carbon ions from the three GCR models considered. This is the free space spectrum at 1 AU outside Earth's magnetosphere.

Table 1. Median and Maximum Absolute Relative Difference for the Three GCR Models Above the Region B Cutoff[a]

	BO2014		DLR		ISO	
	Proton	Carbon	Proton	Carbon	Proton	Carbon
Median absolute relative difference	4.8%	8.1%	3.7%	8.4%	4.5%	8.2%
Maximum absolute relative difference	9.9%	27.1%	12.4%	15.7%	19.6%	42.8%

[a]The results are relative to the average of the three models.

Figure 2 shows model results for both protons and carbon ions over the complete energy grid. All ions were used in the model comparison and transport results; however, protons and carbon ions are used to represent the two major trends in the models. Of the major GCR ions, helium, oxygen, magnesium, and silicon ions all have trends similar to protons. While carbon represents sulfur, calcium, titanium, and iron ions well. Overall, the three models are in agreement at energies above 1 GeV/nucleon.

Due to the Earth's geomagnetic shielding, the high-energy component of the models is the most important when comparing to RaD-X data. Because Figure 2 spans 12 orders of magnitude on the vertical axis, it is difficult to see the differences between the models. Figure 3 shows the high-energy flux scaled by the energy to help flatten the spectrum and make the figure more readable. Above approximately 1.5 GeV, the DLR model predicts slightly larger values of the proton flux compared to the BO2014 model. Above 1.5 GeV, the ISO model predicts the smallest proton flux until near 100 GeV where it tracks very closely with the DLR model and the BO2014 model has the lowest proton flux.

For carbon ions, however, the DLR model predicts larger values compared to BO2014 for all energies between 600 MeV/nucleon and 30 GeV/nucleon. Above 30 GeV/nucleon, the BO2014 predicts the largest flux. The ISO model predicts the smallest flux for carbon ions for all energies but tracks fairly closely with the DLR model above 30 GeV/nucleon.

At low energies, the DLR model has a similar slope to the ISO model but is approximately a factor of 5 larger in flux. Between 10 and 100 MeV/nucleon the DLR model and the BO2014 models increasingly depart from each other with decreasing energy for all ions, with the BO2014 model overpredicting the GCR flux compared to the DLR model. These low-energy differences between the models will not impact the RaD-X comparisons because the low-energy ions do not reach Earth's atmosphere due to the shielding of Earth's geomagnetic field. The average vertical cutoff rigidity for Region B was 3.52 GV, which gives a cutoff energy of 2.70 GeV for protons and 1.06 GeV/nucleon for carbon ions. For Region A, the average vertical cutoff rigidity was 3.81 GV which gives cutoff energies of 2.99 GeV for protons and 1.19 GeV/nucleon for carbon ions.

Table 1 shows the median and maximum absolute relative difference in Region B above the cutoff energy for both protons and carbon ions. Each model was compared to the average flux of the three models at each energy to look at the variation of the models. For protons, the models were very similar and found to have median absolute relative differences in the 4–5% range with maximum absolute relative differences in the 10–20% range. The results for carbon are slightly larger. This is due in large part to the lower cutoff energy for a given cutoff rigidity for ions with charge to mass ratios below that of protons. Median absolute relative differences were about 8% for all three models. The maximum absolute relative differences were, however, larger. Region A had very similar results, and all trends were consistent. The small differences between the models will have a direct effect on the exposures calculated from them.

3. Comparison to RaD-X Dose Measurements

To assess the differences between the GCR models, each boundary flux was used to compute dose rates for Earth's atmosphere conditions corresponding to the RaD-X balloon flight. The RaD-X flight, as discussed above, floated at two different pressures within Earth's atmosphere. Region B, the first part of the flight, was at an average pressure of 4.5 hPa. Region A, the second part of the flight, floated at a higher average pressure of 27.3 hPa. The U.S. standard atmosphere was used to derive average altitude and average atmospheric depth for Regions B and A of the RaD-X flight. The NAIRAS model [*Mertens et al.*, 2013] was used to derive the vertical cutoff rigidities for the two flight segments. An average vertical cutoff rigidity of 3.52 GV and 3.81 GV was calculated for Regions B and A, respectively.

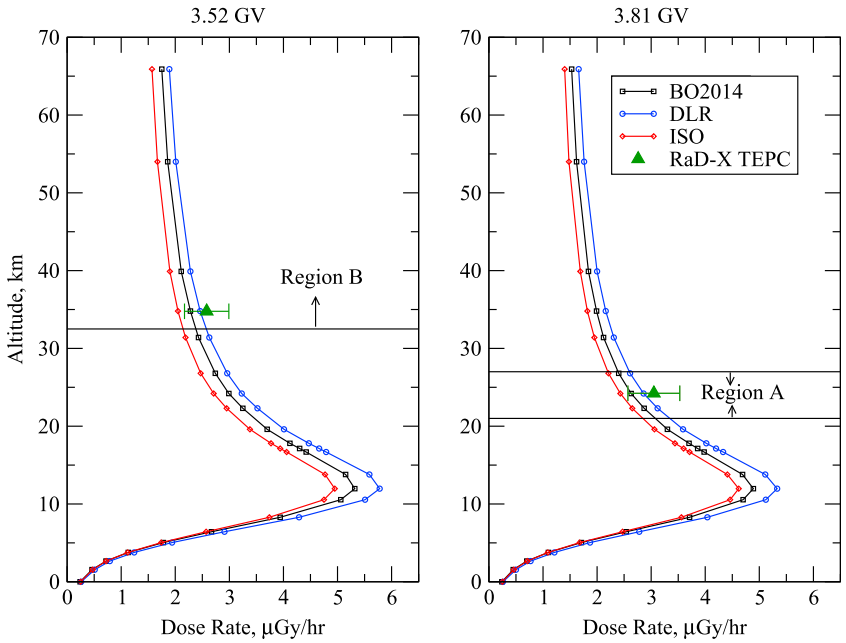

Figure 4. Dose rate in tissue as a function of altitude for the RaD-X flight (25–26 September 2015) from the three GCR models compared to RaD-X TEPC dose rate measurements. (left) Calculated with a vertical cutoff rigidity of 3.52 GV, which corresponds to the average value, while RaD-X was in Region B (> 32.5 km). (right) Calculated with a vertical cutoff rigidity of 3.81 GV, which is the average value during Region A (21–27 km).

The HZETRN transport suite [*Wilson et al.*, 1991] including the effects of pions, muons, electrons, positrons, and photons [*Norman et al.*, 2012, 2013] along with bidirection neutron transport [*Slaba et al.*, 2010a, 2010b] was used to calculate the dose throughout the atmosphere due to the three different GCR boundary fluxes. NAIRAS relies on HZETRN for radiation transport and was therefore a natural choice for this comparison. To emulate the NAIRAS results, HZETRN was run with a single vertical ray in a slab of Earth's atmosphere.

Figure 4 shows the dose rate in tissue as calculated from the previously discussed models as a function of altitude in Earth's atmosphere. The left plot is for a vertical cutoff rigidity of 3.52 GV and right plot for 3.81 GV, which correspond to the value for Regions B and A, respectively. The full atmospheric profile is shown for both regions to illustrate the differences in the same models for Regions B and A, which are due to the differing geomagnetic cutoffs. The small differences in the GCR models show consistent trends in the dose rate. As discussed above, the DLR model, on average, predicted the GCR boundary fluxes as having a higher flux above the vertical cutoff rigidity compared to the other two models, except for carbon, sulfur, calcium, titanium, and iron ions above 30 GeV/nucleon where BO2014 predicted a larger flux. This is consistent with both plots in Figure 4, as the DLR model predicts the largest dose rate at all depths. BO2014 was found to predict larger GCR fluxes than the ISO model, which appears in the exposure calculations as BO2014 predicts higher dose rates than the ISO throughout the atmosphere. Due to the geographic location of the RaD-X flight, the energy regions below 2.7 GeV for protons in the boundary flux did not contribute to the radiation dose and therefore regions where the three models differ most are not included in these results.

The deviation of the three models from the average of the models is largest at the top of the atmosphere for each of the cutoff rigidities, which is about ±10%. The models converge at deeper depths (or lower altitudes), where the spread decreases to approximately ±5%. At small depths, the dose rate will be dominated by the boundary flux as there is not enough atmosphere traversed to significantly alter the radiation field. Deeper in the atmosphere, the secondary particles produced through interaction dominate the dose rate calculation. The three models begin to converge at deeper depths because the particles penetrating to these large depths are created from the very high energy tail of the GCR spectrum. As the three models have more

Table 2. Comparison of the Dose Rate in Tissue Calculated Using the Three GCR Models to RaD-X TEPC Dose Rate Measurements

		TEPC	BO2014	DLR	ISO
Altitude (km)	Pressure (hPa)	Dose Rate (μGy/h)	Dose Rate (μGy/h)	Dose Rate (μGy/h)	Dose Rate (μGy/h)
24.3	27.3	3.05 ± 0.48	2.63	2.86	2.44
36.7	4.5	2.58 ± 0.41	2.28	2.46	2.05

similar spectra at higher energies, it makes sense that the variation in dose rate decreases at large depths since the higher-energy particles are more penetrating. These more penetrating particles will also create more penetrating secondaries.

Table 2 shows the RaD-X TEPC dose rate measurement along with dose rate in tissue calculated using the three GCR models. The TEPC was shown to perform extremely well when compared to National Institute of Standards and Technology-traceable sources during calibration as shown in *Straume et al.* [2016]. For both altitudes, the DLR model provided the boundary flux which came closest to modeling the TEPC dose rate. The DLR model slightly underpredicted the mean TEPC dose rate by a relative error of 5% and 6% in Regions B and A, respectively. The BO2014 model slightly underpredicted the mean TEPC dose rates by a relative error of 12% and 14%, while the ISO model had slightly larger underpredictions of 21% and 20% relative error in Regions B and A, respectively. Both the BO2014 and the DLR models fall within the TEPC dose measurement uncertainty for both altitudes.

The results of comparing the dose rate measured by the silicon-based Liulin detector compared to the dose rate calculated in silicon for the three GCR model boundary fluxes are shown in Table 3. All three GCR models provide a boundary flux that underpredicts the Liulin measurements. The Liulin, however, may be biased high by 30% [*Straume et al.*, 2016]. Compared to the TEPC dose rate, the Liulin dose rate is slightly higher than expected. For the same radiation environment, one would expect the dose in silicon to be lower compared to the dose in tissue due to the differences in stopping power of the two detector materials. In addition, the physical size of the Liulin detector volume creates an upper detection limit 69.4 keV/μm on LET compared to the much larger TEPC with an upper LET limit of 1536 keV/μm. These facts, along with the calibration issue, bring the Liulin measurements on RaD-X into question. The LET spectra from the Liulin and a comparison to the dose measured in silicon from the RaySure instrument may help illuminate the discrepancy.

The DLR model gives the largest predicted dose rate and therefore is the best of the three models for reproducing the Liulin measurements, but the DLR model still underpredicts the mean dose rate in silicon by 27% relative error at the higher altitude and 31% at the lower altitude. The DLR model in Region B is the only model to fall within the Liulin measurement uncertainty for dose.

Figure 5 shows the dose equivalent rate calculated using the three GCR models as a function of altitude compared to the RaD-X TEPC dose equivalent rate measurements. Figure 5 (left) corresponds to Region B and Figure 5 (right) to Region A. The shape of the dose equivalent rate curves calculated from HZETRN using the models is consistent with Figure 6, which shows the RaD-X TEPC dose equivalent rate averaged in a 10 min sliding window as a function of altitude. The models still overpredict the TEPC result, but the shapes are very similar. This is in contrast to the results presented in *Hands et al.* [2016] for the RaySure detector where the dose equivalent rate was flat with altitude above approximately 70,000 ft (~ 21 km) and no local peak was observed.

Table 3. Comparison of the Dose Rate in Silicon Calculated Using the Three GCR Models to RaD-X Liulin Dose Rate Measurements

		Liulin	BO2014	DLR	ISO
Altitude (km)	Pressure (hPa)	Dose Rate (μGy/h)	Dose Rate (μGy/h)	Dose Rate (μGy/h)	Dose Rate (μGy/h)
24.3	27.3	3.42 ± 1.04	2.18	2.36	2.01
36.7	4.5	2.82 ± 0.86	1.89	2.05	1.70

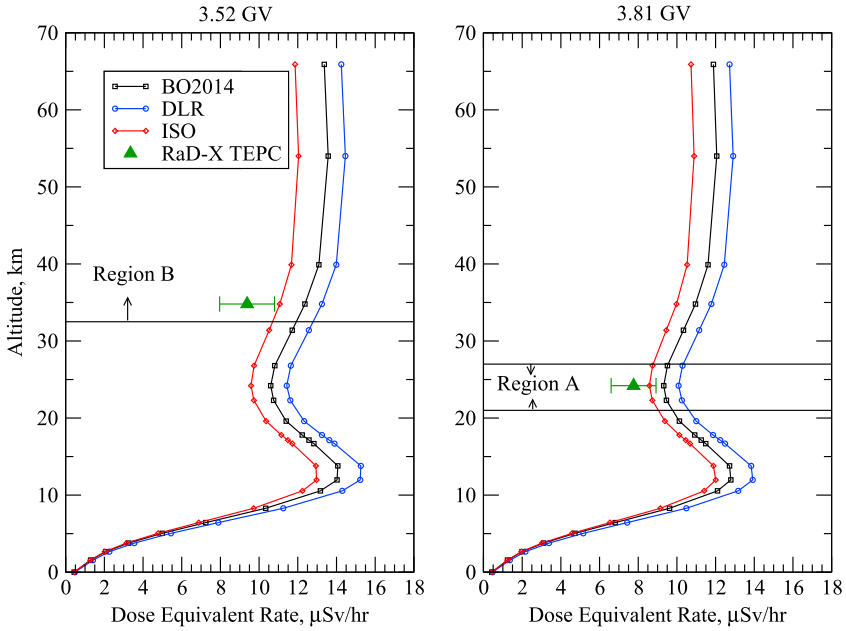

Figure 5. Dose equivalent as a function of altitude for the RaD-X flight (25–26 September 2015) from the three GCR models compared to RaD-X TEPC dose equivalent rate measurements. (left) Calculated with a vertical cutoff rigidity of 3.52 GV, which corresponds to the average value, while RaD-X was in Region B (> 32.5 km). (right) Calculated with a vertical cutoff rigidity of 3.81 GV, which is the average value during Region A (21–27 km).

While the dose rate in tissue was well represented by the models, as discussed above, the dose equivalent rate calculated from all three models overpredicts the TEPC measurement. The dose equivalent rate comparisons seem to be at odds with the dose rate in tissue comparisons. A possible reason for this could be the mix of heavy and light ions predicted by the models compared to the measurements. The average quality factor can give some indication of the mix of heavy to light ions, though it is far from conclusive. Average quality factor $\langle Q \rangle$ is the ratio of the dose equivalent to dose. The quality factor is typically modeled as a particle and LET-dependent quantity representing the ability of a particle at a given LET to damage tissue. Table 4 is a comparison of the average quality factors $\langle Q \rangle$ calculated from the TEPC and using the three GCR models. The GCR models all predict a very similar $\langle Q \rangle$, which is much larger than the value calculated from the TEPC measurements.

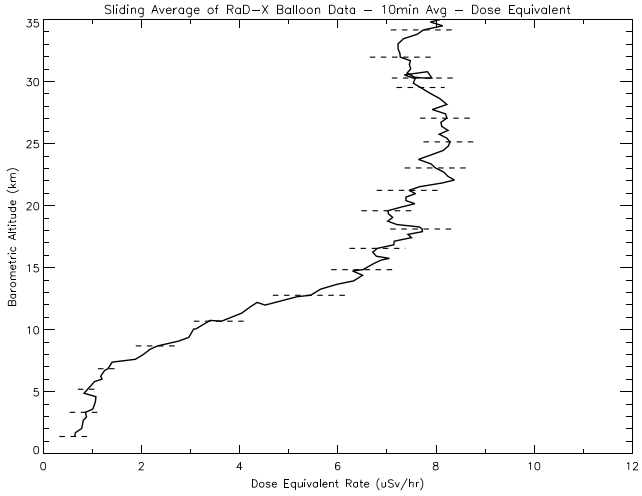

Figure 6. Dose equivalent as a function of altitude for the RaD-X flight (25–26 September 2015) from RaD-X TEPC dose equivalent rate measurements. The TEPC dose equivalent was averaged on a 10 min sliding window.

Table 4. Comparison of the Average Quality Factor Calculated Using the Three GCR Models Compared to the Average Quality Factor Calculated From the TEPC Data

Altitude (km)	Pressure (hPa)	TEPC ($\langle Q \rangle$)	BO2014 ($\langle Q \rangle$)	DLR ($\langle Q \rangle$)	ISO ($\langle Q \rangle$)
24.3	27.3	2.54 ± 0.55	3.54	3.53	3.54
36.7	4.5	3.64 ± 0.80	5.43	5.38	5.40

Figure 7 shows the percent contribution to dose (left) and dose equivalent (right) by particle type for the DLR model with a vertical cutoff rigidity of 3.52 GV. The horizontal dashed magenta lines represent the average altitude in Regions B and A. The values of a given particle correspond to all particles of that type at that altitude, whether they are primary or particles produced through interaction. So, for instance, the protons at all depths, except the very top of the atmosphere, will be a mix of primary GCR protons and protons produced through nuclear interactions.

For Region B (higher altitude), it can be seen that the dose equivalent is dominated by the heavy ions, while at Region A altitudes, the dose equivalent is an even mix of neutrons, hydrogen, helium, and heavy ions. The high value of the quality factor for heavy ions indicates that the flux of heavy ions might be overpredicted at these altitudes. In addition, it has been shown recently by *Ehresmann et al.* [2014] that HZETRN overpredicts the flux of helium isotopes in Mars atmosphere. As helium also has a fairly large quality factor, it may also be contributing to the overprediction of dose equivalent.

A large contribution to the likely incorrect influence of heavy ions at these small depths in the atmosphere is the use of a single ray transport in HZETRN. The inclusion of off-axis rays to the transport would reduce the flux of heavy ions and likely reduce the average quality factor and dose equivalent. An additional factor, though one that is probably not as important for Region B, is the calculation of the dose equivalent from neutrons in HZETRN. This calculation relies on older quality factors for neutrons which are slightly higher than the current standards.

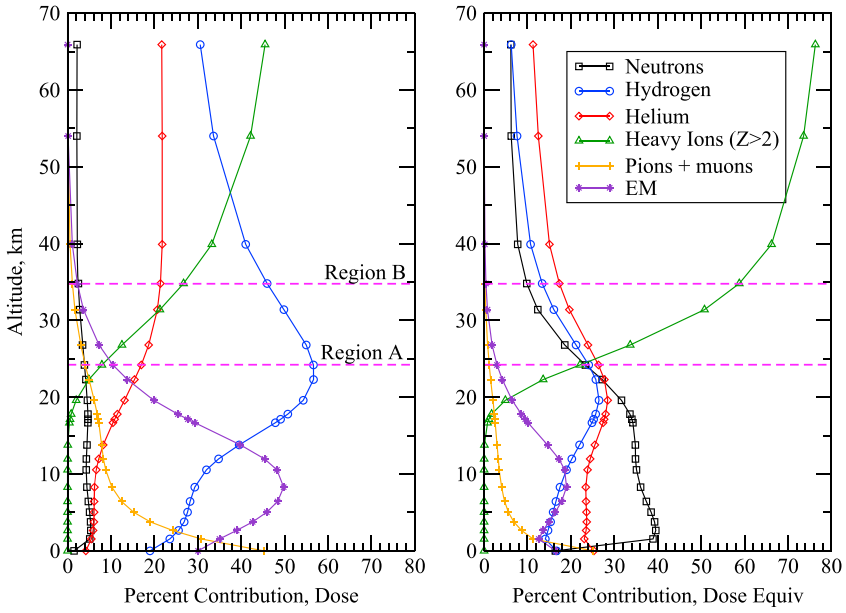

Figure 7. The percent contribution to (left) dose and (right) dose equivalent by different particle groups as a function of altitude for the RaD-X flight (25–26 September 2015) from the three GCR models. Horizontal dashed lines correspond to average altitude for Regions B and A for reference.

4. Concluding Remarks

RaD-X data provide a good test of the GCR models used in radiation transport codes and are an important source for validation of the NAIRAS model. This paper examined three GCR models, the parametric ISO 15390 model, the DLR model, which is a modification to the ISO model, and the Badhwar-O'Neill 2014 model. Differences between the three models were examined, and results were shown for the dates of the RaD-X flight. Low-energy cosmic ray particles, whose fluxes vary widely between the models, are of little consequence to the dose calculations and the RaD-X measurements because the geomagnetic field shields against these low-energy particles. The fact that the geomagnetic cutoff for the flight path was found to be so high that it removed the major differences between the GCR models creates the argument for the need for additional data at higher latitudes where the geomagnetic cutoffs are smaller.

The differences in the GCR boundary flux provided by the three GCR models translated into small differences in the radiation dose calculated from those three boundary fluxes. The DLR model was found to match the dose in tissue results most closely, with only a 5% relative difference in Region B and a 6% relative difference in Region A. The BO2014 was next in accuracy compared to the TEPC measurements, followed by the ISO model. The ISO model was released in 2004 and has not been updated since. A similar update to the work done with the DLR model or with BO2014 would be appropriate.

When the three models were compared to the Liulin instrument that measures the dose in silicon, the models were found to all underpredict the measurement. The reported dose rate in silicon from the Liulin seems to be slightly higher than expected compared to the TEPC results. One would expect the dose in silicon to be lower than the dose in tissue, as silicon absorbs less energy than tissue due to the smaller average stopping power of silicon compared to tissue. However, the Liulin measured dose in silicon to be very nearly the same as the TEPC measured dose in tissue. In addition, the small size of the Liulin detector creates an upper limit for the LET sensitivity of 69.4 keV/μm, while the TEPC is able to measure up to 1536 keV/μm. The differences in material and detector size both support the notion that the Liulin should measure a dose lower than the TEPC in the upper atmosphere. *Straume et al.* [2016] found that the Liulin may be biased high by 30%, so the calibration studies using the same instruments are consistent with the measurement results.

Next, the TEPC dose equivalent rate was compared to the dose equivalent rate calculated from the three GCR models. The three GCR models all predicted a dose equivalent rate that was larger than the TEPC dose equivalent rate. Given the accuracy of the three GCR models compared to measurements of dose rate in tissue, the overprediction of dose equivalent may point to an issue with the mix of heavy ions, light ions, protons, and neutrons. When the average quality factor was examined, it was found that the value calculated from the three GCR models was about 50% high compared to the TEPC measurements.

The issue of the contribution of heavy ions also shows up in measurements when comparing different detectors. *Hands et al.* [2016] saw no evidence for primary heavy ions contributing to dose equivalent at any depth using the RaySure detector. While in Figure 6, it can be seen that the mean dose equivalent in Regions B and A is different. In addition, a decrease in dose equivalent rate with increasing depth in Region B points to the breakup of the primary spectrum. However, when the uncertainties are included, the analysis is not conclusive. The difference between the average quality factor for the TEPC in Regions B and A also points to the breakup of the primary heavy ions. Further analysis examining the LET spectra from the instruments would help to clarify and resolve this issue.

As all of these measurements are integrated quantities, the source of differences between model and experiment cannot be determined directly from this information. Further work comparing to particle flux in Earth's atmosphere will be performed to better understand the source of the discrepancy. In addition, the single ray used in the calculation with HZETRN coupled with the larger average quality factor signals that future modeling work needs to be done to include the contribution of off-axis rays.

Using the RaD-X data to propagate model uncertainty through NAIRAS to quantify the component of the uncertainty due to the GCR model is an ongoing effort. Uncertainty propagation methods are being developed, which will use not only RaD-X data but will also make use of other data sources in Earth's upper atmosphere.

Acknowledgments
The authors acknowledge the support from the NASA Science Mission Directorate under the Hands-On Project Experience (HOPE-4) opportunity, which was the principal source of funding for the RaD-X balloon flight mission. The authors wish to thank the Sodankyla Geophysical Observatory which provided the Oulu neutron monitor count rates through their website http://cosmicrays.oulu.fi. All other data can be found in the figures, tables, and references. All data are available from the authors by request.

References

Aguilar, M., et al. (2015), Precision measurement of the proton flux in primary cosmic rays from rigidity 1 GV to 1.8 TV with the Alpha Magnetic Spectrometer on the International Space Station, *Phys. Rev. Lett.*, *114*, 171103, doi:10.1103/PhysRevLett.114.171103.

Clette, F., L. Svalgaard, J. M. Vaquero, and E. W. Cliver (2014), Revisiting the sunspot number, *Space Sci. Rev.*, *186*(1), 35–103, doi:10.1007/s11214-014-0074-2.

Copeland, K., H. H. Sauer, F. E. Duke, and W. Friedberg (2008), Cosmic radiation exposure of aircraft occupants on simulated high-latitude flights during solar proton events from 1 January 1986 through 1 January 2008, *Adv. Space Res.*, *42*(6), 1008–1029, doi:10.1016/j.asr.2008.03.001.

Dachev, T., P. Dimitrov, B. Tomov, Y. Matviichuk, F. Spurny, O. Ploc, K. Brabcova, and I. Jadrnickova (2011), Liulin-type spectrometry-dosimetry instruments, *Radiat. Prot. Dosimetry*, *144*(1–4), 675–679, doi:10.1093/rpd/ncq506.

Dyer, C., A. Hands, F. Lei, P. Truscott, K. A. Ryden, P. Morris, I. Getley, L. Bennett, B. Bennett, and B. Lewis (2009), Advances in measuring and modeling the atmospheric radiation environment, *IEEE Trans. Nucl. Sci.*, *56*(6), 3415–3422, doi:10.1109/TNS.2009.2032185.

Ehresmann, B., et al. (2014), Charged particle spectra obtained with the Mars Science Laboratory Radiation Assessment Detector (MSL/RAD) on the surface of Mars, *J. Geophys. Res. Planets*, *119*, 468–479, doi:10.1002/2013JE004547.

Hands, A. D. P., K. Ryden, and C. J. Mertens (2016), The disappearance of the Pfotzer-Regener maximum: Dose equivalent measurements in the stratosphere, *Space Weather*, *14*, doi:10.1002/2016SW001402.

International Commission on Radiological Protection (1991), 1990 Recommendations of the International Commission on Radiological Protection, *ICRP Publ., Rep. No. 60*.

International Commission on Radiological Units (ICRU) (1992), International Commission of Radiation Units and Measurements, Measurement of dose equivalents from external photon and electron radiations, *ICRU Rep. No. 47*.

International Commission on Radiological Units (ICRU) (2001), International Commission of Radiation Units and Measurements, Determination of operational dose-equivalent quantities for neutrons, *ICRU Rep. No. 66*.

International Commission on Radiological Units (ICRU) (2010), International Commission of Radiation Units and Measurements, Reference data for the validation of doses from cosmic-radiation exposure of aircraft crew, *ICRU Rep. No. 84*.

International Organization for Standardization (ISO) (2004), *Space Environment (Natural and Artificial)—Galactic Cosmic Ray Model, Standard*, International Organization for Standardization, Geneva, Switzerland.

Lindborg, L., D. Bartlett, P. Beck, I. McAulay, K. Schnuer, H. Schraube, and F. Spurny (2004), Cosmic radiation exposure of aircraft crew: Compilation of measured and calculated data, *Radiat. Prot. Dosimetry*, *110*(1–4), 417–422, doi:10.1093/rpd/nch232.

Matthiä, D., T. Berger, A. I. Mrigakshi, and G. Reitz (2013), A ready-to-use galactic cosmic ray model, *Adv. Space Res.*, *51*(3), 329–338, doi:10.1016/j.asr.2012.09.022.

Mertens, C. J., B. T. Kress, M. Wiltberger, S. R. Blattnig, T. S. Slaba, S. C. Solomon, and M. Engel (2010), Geomagnetic influence on aircraft radiation exposure during a solar energetic particle event in October 2003, *Space Weather*, *8*, S03006, doi:10.1029/2009SW000487.

Mertens, C. J., B. T. Kress, M. Wiltberger, W. K. Tobiska, B. Grajewski, and X. Xu (2012), Atmospheric ionizing radiation from galactic and solar cosmic rays, in *Current Topics in Ionizing Radiation Research*, edited by M. Nenoi, Intech, Rijeka, Croatia.

Mertens, C. J., M. M. Meier, S. Brown, R. B. Norman, and X. Xu (2013), NAIRAS aircraft radiation model development, dose climatology, and initial validation, *Space Weather*, *11*, 603–635, doi:10.1002/swe.20100.

Mrigakshi, A. I., D. Matthiä, T. Berger, G. Reitz, and R. F. Wimmer-Schweingruber (2013), How galactic cosmic ray models affect the estimation of radiation exposure in space, *Adv. Space Res.*, *51*(5), 825–834, doi:10.1016/j.asr.2012.10.017.

National Council on Radiation Protection and Measurements (NCRP) (2006), National council on radiation protection and measurements, information needed to make radiation protection recommendations for space missions beyond low-earth orbit, *NCRP Rep. No. 153*.

National Council on Radiation Protection and Measurements (NCRP) (2009), National council on radiation protection and measurements, ionizing radiation exposure of the population of the United States, NCRP Rep. No. 160.

Norman, R. B., S. R. Blattnig, G. De Angelis, F. F. Badavi, and J. W. Norbury (2012), Deterministic pion and muon transport in Earth's atmosphere, *Adv. Space Res.*, *50*(1), 146–155, doi:10.1016/j.asr.2012.03.023.

Norman, R. B., T. C. Slaba, and S. R. Blattnig (2013), An extension of HZETRN for cosmic ray initiated electromagnetic cascades, *Adv. Space Res.*, *51*(12), 2251–2260, doi:10.1016/j.asr.2013.01.021.

Nymmik, R., and A. Suslov (1995), Characteristics of galactic cosmic ray flux lag times in the course of solar modulation, *Adv. Space Res.*, *16*(9), 217–220, doi:10.1016/0273-1177(95)00338-F.

Nymmik, R., M. Panasyuk, and A. Suslov (1996), Galactic cosmic ray flux simulation and prediction, *Adv. Space Res.*, *17*(2), 19–30, doi:10.1016/0273-1177(95)00508-C.

O'Neill, P. M., S. Golge, and T. C. Slaba (2015), Badhwar-O'Neill 2014 galactic cosmic ray flux model description, NASA TP-2015-218569.

Ploc, O., I. Ambrozova, J. Kubancak, I. Kovar, and T. P. Dachev (2013), Publicly available database of measurement with the silicon spectrometer Liulin on board aircraft, *Radiat. Meas.*, *58*, 107–112, doi:10.1016/j.radmeas.2013.09.002.

Regener, E., and G. Pfotzer (1934), Intensity of the cosmic ultra-radiation in the stratosphere with the tube-counter, *Nature*, *134*, 325, doi:10.1038/134325b0.

Slaba, T., S. Blattnig, and F. Badavi (2010a), Faster and more accurate transport procedures for HZETRN, *J. Comput. Phys.*, *229*(24), 9397–9417, doi:10.1016/j.jcp.2010.09.010.

Slaba, T., S. Blattnig, S. Aghara, L. Townsend, T. Handler, T. Gabriel, L. Pinsky, and B. Reddell (2010b), Coupled neutron transport for HZETRN, *Radiat. Meas.*, *45*(2), 173–182, doi:10.1016/j.radmeas.2010.01.005.

Slaba, T. C., and S. R. Blattnig (2014a), GCR environmental models I: Sensitivity analysis for GCR environments, *Space Weather*, *12*(4), 217–224, doi:10.1002/2013SW001025.

Slaba, T. C., and S. R. Blattnig (2014b), GCR environmental models II: Uncertainty propagation methods for GCR environments, *Space Weather*, *12*, 225–232, doi:10.1002/2013SW001026.

Slaba, T. C., X. Xu, S. R. Blattnig, and R. B. Norman (2014), GCR environmental models III: GCR model validation and propagated uncertainties in effective dose, *Space Weather*, *12*, 233–245, doi:10.1002/2013SW001027.

Stone, E., A. Frandsen, R. Mewaldt, E. Christian, D. Margolies, J. Ormes, and F. Snow (1998), The advanced composition explorer, *Space Sci. Rev.*, *86*(1), 1–22, doi:10.1023/A:1005082526237.

Straume, T., C. J. Mertens, T. C. Lusby, B. Gersey, W. K. Tobiska, R. B. Norman, G. P. Gronoff, and A. Hands (2016), Ground-based evaluation of dosimeters for NASA high-altitude balloon flight, *Space Weather*, *14*, doi:10.1002/2016SW001402.

Wilson, J. W., L. W. Townsend, W. Schimmerling, G. S. Khandelwal, F. Khan, J. E. Nealy, F. A. Cucinotta, L. C. Simonsen, J. L. Shinn, and J. W. Norbury (1991), Transport methods and interactions for space radiations, NASA RP-1257.